Journal of Alloys and Compounds 969 (2023) 172385

Contents lists available at ScienceDirect

Journal of Alloys and Compounds

journal homepage: www.elsevier.com/locate/jalcom

Structure and dielectric properties in Mg/Nb co-substituted bismuth sodium titanate

Hangfeng Zhang [a,b], Haixue Yan [b,*], Isaac Abrahams [a,*]

[a] Department of Chemistry, Queen Mary University of London, Mile End Road, London E1 4NS, UK
[b] School of Engineering and Materials Science, Queen Mary University of London, Mile End Road, London E1 4NS, UK

ARTICLE INFO

Keywords:
Bismuth sodium titanate
Mg,Nb co-doping
Ferroelectric

ABSTRACT

A systematic study of pseudo-isovalent B site co-substitution of Ti^{4+} by Mg^{2+} and Nb^{5+} in bismuth sodium titanate is presented. A complete solid solution in the $Bi_{0.5}Na_{0.5}Ti_{1-x}(Mg_{1/3}Nb_{2/3})_xO_3$ system is formed. With increasing level of substitution, dielectric anomalies associated with depoling and maximum permittivity temperatures (T_d and T_m, respectively) are suppressed and shift to lower temperatures. Variable temperature X-ray powder diffraction on the $x = 0.2$ composition reveals a non-linear thermal expansion at temperatures below T_m. B-site co-substitution by Mg and Nb has the effect of interrupting the long-range ferroelectric ordering in the system, resulting in lower saturation and remnant polarizations. A maximum energy storage density of 4.14 J cm^{-3} with a recoverable energy density of 2.35 J cm^{-3} was obtained for the $x = 0.1$ composition, while the $x = 0.5$ composition appears to have the best balance between energy storage and energy efficiency.

1. Introduction

With the rapid development of electronic technology in portable electronic devices, medical equipment, and electric vehicles [1], high power energy storage capacitors have become ubiquitous. Lead containing dielectric capacitors, based on ferroelectric materials such as lead zirconium titanate ($PbZr_xTi_{1-x}O_3$, PZT) [2], show excellent performance characteristics, but there is now an urgent need to replace these with lead-free systems due to concerns over toxicity and environmental pollution during manufacture [3]. The properties of PZT compositions at the morphotropic phase boundary (MPB) between tetragonal and rhombohedral phases represent the benchmark for piezoelectric applications [4]. The similar free energies of the two phases leads to their co-existence and enhanced polarizability under DC electrical poling. Over the last two decades, relaxor type ferroelectric materials with MPBs, such as $PbTi_{1-x}(Mg_{1/3}Nb_{2/3})_xO_3$ (PMN-PT) [5] and $PbTi_{1-x}(Zn_{1/2}Nb_{2/3})_xO_3$ (PZN-PT) [6], have shown extraordinary performance with ultrahigh piezoelectric coefficients, d_{33} (> 2500 pC N^{-1}), and electromechanical strain coupling, k_{33} (> 0.9) [4].

Bismuth sodium titanate ($Bi_{0.5}Na_{0.5}TiO_3$, BNT) based relaxor ferroelectric materials exhibit very favorable characteristics for high power energy storage in capacitors, due to their narrow polarization-electric field (*P-E*) hysteresis loops with large saturation polarization under high electric fields [7,8]. BNT based ceramics have become the focus of much research as lead-free alternatives to lead-based materials. There have been numerous studies on A site substitution in BNT, with far less exploring the possibility of B-site substitution. B-site substitution in BNT of Ti^{4+} by the isovalent Zr^{4+} ion leads to a solid solution of general formula $Bi_{0.5}Na_{0.5}Ti_{1-x}Zr_xO_3$ (BNTZ) [9], with compositions in the range $0.0 \leq x \leq 0.2$ formed of mixtures of both rhombohedral (space group *R*3*c*) and monoclinic (space group *Cc*) phases. Pseudo-isovalent substitution for Ti^{4+} can be achieved using a combination of subvalent and supervalent ions as in the PMN-*x*PT system, i.e., $PbTi_{1-x}(Mg_{1/3}Nb_{2/3})_xO_3$ [5,10], where a complete solid solution is observed, despite the fact that the ionic radii of Mg^{2+} and Nb^{5+} are both slightly larger than that of Ti^{4+}. No similar studies have been carried out in BNT based systems. Such co-substitution strategies can lead to greater disorder and higher values of configurational entropy, which can help in the stabilization of high symmetry structures.

In the present work, the effects on dielectric properties of magnesium and niobium co-substitution for titanium on the B site of BNT is investigated in compositions of general formula $Bi_{0.5}Na_{0.5}Ti_{1-x}(Mg_{1/3}Nb_{2/3})_xO_3$ (BNTMN). Co-substitution of divalent Mg^{2+} and pentavalent Nb^{5+} in a 1:2 ratio for tetravalent Ti^{4+} in BNT represents an overall isovalent substitution and therefore no further charge compensation is required to maintain electroneutrality, minimizing the chance of oxide ion vacancy

* Corresponding authors.
E-mail addresses: h.x.yan@qmul.ac.uk (H. Yan), i.abrahams@qmul.ac.uk (I. Abrahams).

https://doi.org/10.1016/j.jallcom.2023.172385
Received 27 March 2023; Received in revised form 26 June 2023; Accepted 1 October 2023
Available online 5 October 2023

creation, which could lead to high dielectric loss. In addition, co-substitution is predicted to increase disorder on the B-site and in doing so reduce remnant polarization and hence increase efficiency. B-site substitution in this system is found to greatly improve the energy storage performance of BNT, with BNTMN ceramics found to have relatively high energy density with good energy efficiency.

2. Experimental

Compositions of general formula $Bi_{0.5}Na_{0.5}Ti_{1-x}(Mg_{1/3}Nb_{2/3})_xO_3$ (x = 0.1, 0.2, 0.35, 0.5, 0.8 and 1.0) were prepared by conventional solid-state synthesis in two steps. The first step was the synthesis of $MgNb_2O_6$ to be used as a precursor. Stoichiometric amounts of $(MgCO_3)_4{\cdot}Mg(OH)_2{\cdot}5\ H_2O$ (Aldrich, 99.99%) and Nb_2O_5 (Aldrich, 99.9%), were ground in ethanol with a planetary ball mill (QM-3SP4, Nanjing University Instrument Plant, China), using a nylon jar with zirconia balls, at 360 rpm for 4 h. The resulting slurry was dried on a hot plate at 150 °C and sieved through a 250 μm sieve. The powder was then heated at 1250 °C for 4 h to form $MgNb_2O_6$ in an alumina crucible. In the second step stoichiometric amounts of $MgNb_2O_6$, Na_2CO_3 (Alfa Aesar, 99.5%, pre-heated at 200 °C for 24 h), Bi_2O_3 (Aldrich, 99.9%), and TiO_2 (Aldrich, 99.8%), were ball milled at 360 rpm for 4 h in ethanol. The resulting slurry was dried and sieved and the powder heated to 840 °C for 4 h in an alumina crucible. After cooling, the powder was ball milled again in ethanol at 360 rpm for 4 h, followed by drying and sieving. The powder was then pressed uniaxially at ca. 150 MPa into pellets of 15 mm diameter and ca. 1 mm thickness and sintered at 1150 °C for 3 h to form the final ceramics.

The surface morphology of samples was observed using scanning electron microscopy (FEI Inspect F SEM). Samples for SEM characterizations were coated with gold. The incident beam was generated at 30 kV. X-ray powder diffraction (XRD) data were collected on a PANalytical X'Pert Pro diffractometer using Ni-filtered Cu-Kα radiation (λ = 1.5418 Å). Data were collected at room temperature in flat plate θ/θ geometry over the 2θ range 5 − 120°, with a step width of 0.0334° and an effective count time of 50 s per step. Data were modelled by Rietveld analysis using the GSAS suite of programs [11]. Structure refinement was carried out using an ideal perovskite model in space group *Pm*-3*m* [12]. Raman scattering spectra were collected on $Bi_{0.5}Na_{0.5}Ti_{1-x}(Mg_{1/3}Nb_{2/3})_xO_3$ ceramics using a ViaTM confocal Raman microscope with a 633 nm wavelength laser.

For dielectric measurements, sintered pellets were ground into plates of dimensions ca. 4 × 4 × 0.3 mm^3 and polished. The parallel surfaces of the plates were coated with silver paste (Gwent Electronic Materials Ltd., C2011004D5, Pontypool, UK) and heated at 250 °C to form a conductive layer. A precision impedance analyzer (Agilent 4294 A) was used to measure the dielectric permittivity and loss over the frequency range 100 Hz to 1 MHz. Temperature dependent measurements were made in a tube furnace using an Agilent 4284 A LCR meter. Ferroelectric current-electric field (*I-E*) and polarization-electric field (*P-E*) loops were measured at room temperature using a ferroelectric hysteresis measurement tester (NPL, UK), with voltage applied in a triangular waveform [13].

3. Results and discussion

The XRD patterns of the studied compositions are shown in Fig. 1a. In all cases, the main diffraction peaks were well fitted in space group *Pm*-3*m* (Fig. S1), using an ideal perovskite model, with A site atoms located at 0, 0, 0, B atoms at ½, ½, ½ and O at ½, ½, 0. Crystal and refinement parameters are summarized in Table S1. For compositions $x = 0.8$ and $x = 1.0$, additional peaks are observed and exhibit a higher intensity in the latter composition (marked by solid circles in Fig. 1a). The peaks for the secondary phase match those for $Bi_{1.66}Mg_{0.7}Nb_{1.52}O_7$, which possesses a pyrochlore structure in space group *Fd*-3*m* [14]. The weight fraction of the secondary phase was 9.2% and 15.2% for compositions $x = 0.8$ and $x = 1.0$, respectively. However, the exact stoichiometry of this secondary phase cannot be confirmed. The unit cell volume of the BNT-*x*MN system shows an almost linear increase with increasing *x*-value (Fig. 1b). This is consistent with the smaller Ti^{4+} (r = 0.605 Å, for 6-coordinate geometry [15]) being replaced by the larger Mg^{2+} and Nb^{5+} cations with an average radius of 0.67 Å for $(Mg_{1/3}Nb_{2/3})^{4+}$. The linear variation of unit cell volume with composition suggests a complete solid solution in accordance with Vegard's law, despite the appearance of a secondary phase at $x = 0.8$. This apparently sodium deficient secondary phase suggests a degree of sodium volatilization, resulting in the appearance of the pyrochlore phase at higher levels of substitution. A similar problem was reported in the preparation of $PbTi_{1-x}(Mg_{1/3}Nb_{2/3})_xO_3$, where a pyrochlore phase was also observed at higher *x*-values [16]. The morphology of the studied compositions was examined by SEM (Fig. S2). Fractured surface scans reveal transgranular fracture, indicative of stronger bonding in grain boundaries than in grains. The grain size increases from ca. 5 μm for the $x = 0.1$ composition to ca. 15 μm at $x = 1.0$.

Fig. 2 shows the Raman spectra of the studied compositions measured at room temperature. All compositions shows similar Raman spectra to those of other BNT based materials [17–21]. The broad peaks in the spectra are attributed to the structural disorder induced by the random distribution of cations in both A (Bi/Na) and B (Ti/Mg/Nb) sites. For BNT based materials, the Raman modes can be divided into

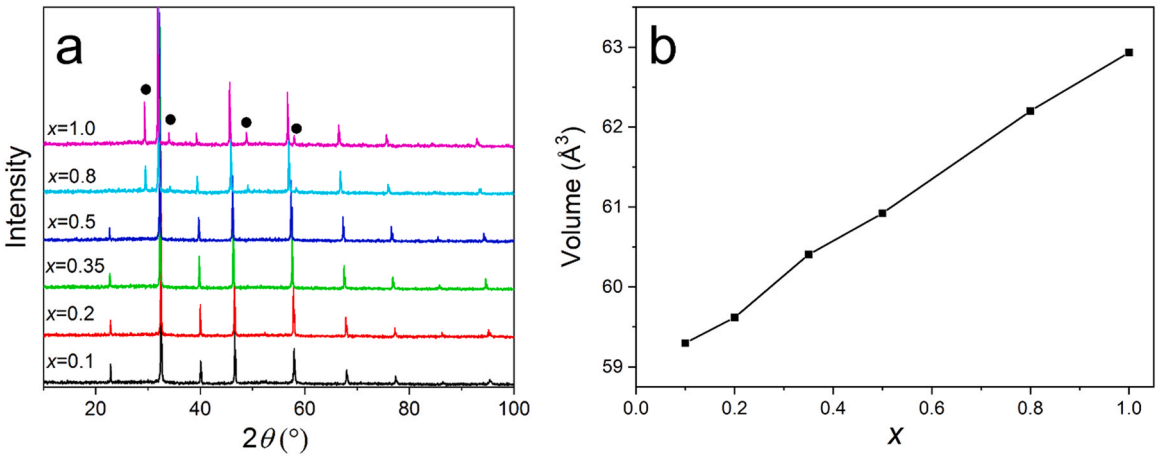

Fig. 1. (a) XRD patterns of the studied compositions and (b) compositional variation of unit cell volume in the $Bi_{0.5}Na_{0.5}Ti_{1-x}(Mg_{1/3}Nb_{2/3})_xO_3$ system. Solid circles in (a) indicate reflections of a secondary pyrochlore phase. Error bars in (b) are smaller than the symbols used.

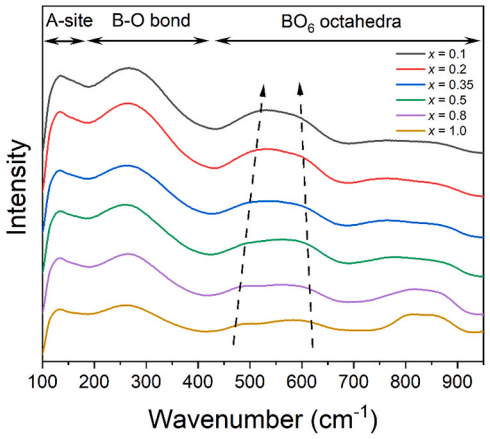

Fig. 2. Raman spectra of $Bi_{0.5}Na_{0.5}Ti_{1-x}(Mg_{1/3}Nb_{2/3})_xO_3$ ceramic samples.

three distinct regions: A-site vibrations (< 200 cm^{-1}), B-O vibrations (200–400 cm^{-1}) and BO_6 vibrations (400–700 cm^{-1}) including breathing and stretching modes. The peaks associated with the BO_6 vibration modes widen with increasing *x*-value which can be attributed to the increased disorder induced by double substitution at the B-site.

The frequency dependencies of room temperature dielectric permittivity and loss tangent of the studied compositions are shown in Fig. 3. All samples reveal a slight decrease in dielectric permittivity at higher frequency. In dielectric materials, various polarization mechanisms contribute to the overall permittivity. When the frequency increases, the dielectric response of the material to the external electric field becomes slower due to the relaxation time of the dipoles. The reduction in permittivity at higher frequencies is associated with this relaxation process [22]. In all compositions, the loss tangent increases with frequency, but with relatively low values. Although the XRD analysis indicates an average non-polar structure, the changes in dielectric permittivity and loss with frequency, suggest the presence of local polar regions [23]. The increase in loss tangent with frequency is likely due to the different polar regions associated with different relaxation times [24,25]. The dielectric permittivity of the studied compositions decreases with increasing x-value, which suggests that Mg^{2+} and Nb^{5+} substitution in the $Bi_{0.5}Na_{0.5}Ti_{1-x}(Mg_{1/3}Nb_{2/3})_xO_3$ system stabilizes the non-polar structure and reduces the concentration of local polar regions.

Fig. 4 shows the temperature dependencies of dielectric permittivity and loss at different frequencies. The dielectric loss tangent is a measure of the dissipation of electrical energy and is calculated from the ratio of the imaginary and real parts of complex dielectric permittivity. As the temperature increases, the loss tangent generally shows a variation due to changes in the structure and conductivity of the material, as well as

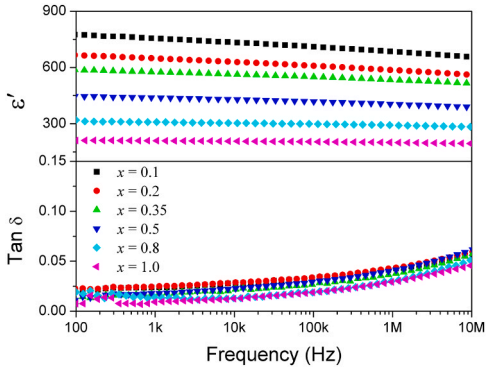

Fig. 3. Frequency dependencies of dielectric permittivity and loss for the studied compositions in the $Bi_{0.5}Na_{0.5}Ti_{1-x}(Mg_{1/3}Nb_{2/3})_xO_3$ system.

the activation energy of polarization processes [26]. For the $x = 0.1$ composition, two anomalies are observed at ca. 200 °C and 350 °C. The higher temperature anomaly corresponds to the temperature of maximum permittivity (T_m), while the low temperature anomaly is tentatively attributed to the depolarization temperature, T_d, above which spontaneous long-range ferroelectric polarization vanishes [27]. Both T_d and T_m shift to lower temperature and become less pronounced as *x* increases and are hardly distinguishable at $x = 0.5$. At temperatures below T_d, the diffuse nature of the dielectric permittivity is due to the formation of a larger range of local polar regions with different activation energies [28,29]. At temperatures between T_d and T_m, the local polar regions are relatively small and exhibit similar relaxation behavior to each other resulting in frequency independent dielectric permittivity. At temperatures above T_m, the diffuseness in the dielectric response reappears due to thermally induced electronic conductivity at high temperatures, with a resultant increase in dielectric loss [30]. For the $x = 0.8$ and 1.0 compositions, T_d and T_m are not observable, consistent with these compositions being present predominantly as the paraelectric cubic phase.

To further investigate the anomalies associated with T_d and T_m, variable temperature X-ray diffraction was carried out for the $x = 0.2$ composition (Fig. S3). No obvious additional peaks or peak splitting occurred over the measured temperature range to indicate phase transitions associated with these anomalies. The unit cell volume generally increases with increasing temperature (Fig. 5), but the plot shows a degree of curvature at temperatures above 300 °C which coincides with T_m. Although the average structure of the $(Bi_{0.5}Na_{0.5}TiO_3)_{1-x}(Ba_{0.4}Sr_{0.6}TiO_3)_x$ system is non-polar and cubic, randomly oriented polar nano-regions can exist embedded in the cubic matrix as seen in other BNT based systems [12,31–33]. As temperature increases from T_d to T_m, the ordering in the polar regions breaks down, leading to a greater number of polar nano-regions being formed with a consequent increase in volume to accommodate the increased disorder. This type of non-linear volume expansion in the pseudo-cubic structure has been observed in other relaxor ferroelectrics such as the $(Bi_{0.5}Na_{0.5}TiO_3)_{1-x}(Ba_{0.4}Sr_{0.6}TiO_3)_x$ system [12] and $PbMn_{0.33}Nb_{0.67}O_3$ (PMN), where the increasing thermal expansion was attributed to a decrease in electrostriction and polarization [34].

Fig. 6 shows room temperature *I-E* and *P-E* loops for the studied compositions in the $(Bi_{0.5}Na_{0.5}TiO_3)_{1-x}(Ba_{0.4}Sr_{0.6}TiO_3)_x$ system at high electric field. With decreasing value of *x*, higher values of saturation polarization and remnant polarization are observed. The *P-E* loops show a gradual narrowing with increasing *x*-value, becoming almost linear at $x = 0.8$, indicating a weakening of ferroelectric behavior with increasing Mg/Nb content. At $x = 0.1$, four broad current peaks are observed in the *I-E* loop, which gradually vanish as *x* increases and are totally absent at $x = 0.8$. These current peaks occur in all four quadrants of the *I-E* loop at $x = 0.1$ and are consistent with a field induced reversible phase transition, as seen in other BNT based materials [12, 35–39]. For the $x = 0.1$ and 0.2 compositions, which have T_d values above room temperature, the polar regions are partially stabilized after removal of the electric field, resulting in some remanent polarization in the respective *P-E* loops.

The total energy density, u_{total}, energy loss, u_{loss}, and energy efficiency, η, of the studied compositions were calculated using the following equations [40].

$$u_{total} = \int_{P_0}^{P_{max}} E dP \quad (1)$$

$$u_{loss} = \int_{P_{remanant}}^{P_{max}} E dP \quad (2)$$

$$\eta = 1 - \frac{u_{loss}}{u_{total}} \quad (3)$$

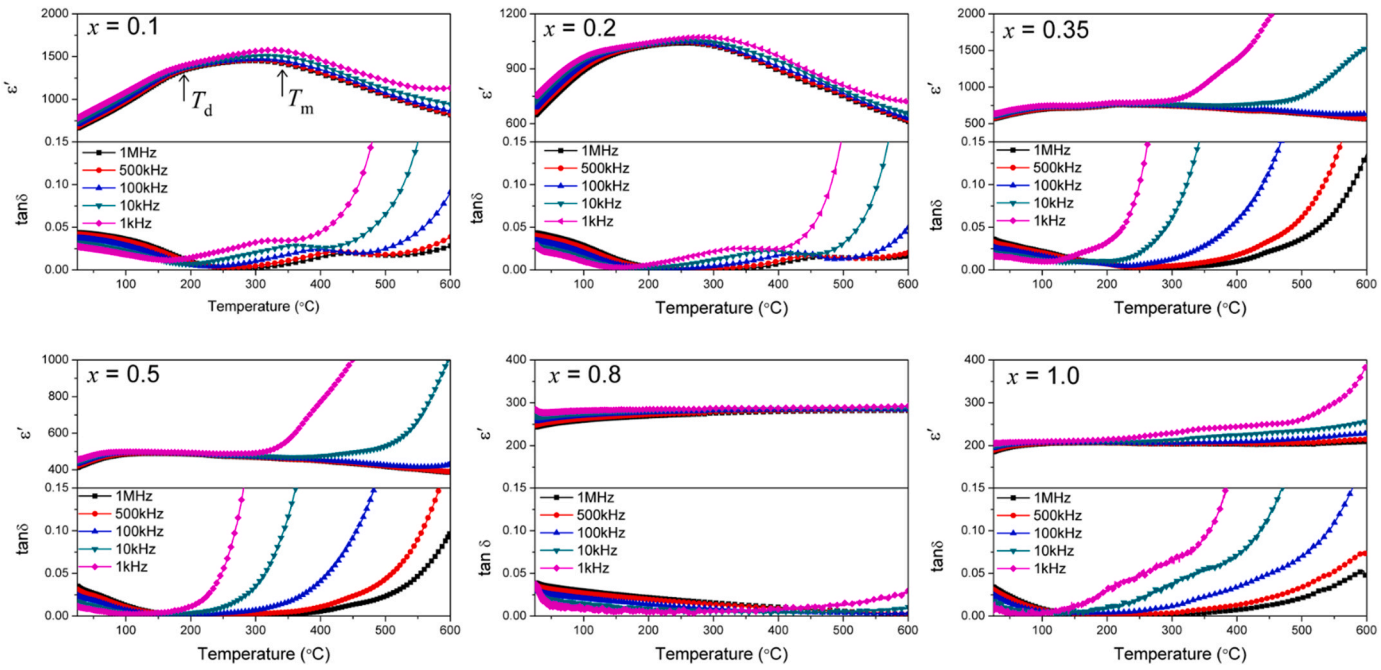

Fig. 4. Temperature dependencies of dielectric permittivity and loss for the studied compositions in the $Bi_{0.5}Na_{0.5}Ti_{1-x}(Mg_{1/3}Nb_{2/3})_xO_3$ system.

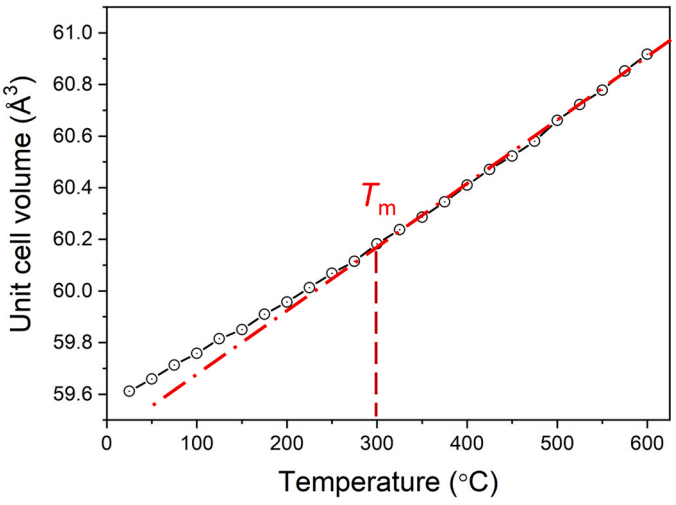

Fig. 5. Temperature dependence of unit cell volume in $Bi_{0.5}Na_{0.5}Ti_{0.8}(Mg_{1/3}Nb_{2/3})_{0.2}O_3$.

where E is the applied field and P is the polarization. Compositions $x = 0.35$ and 0.50 show values of 0.209 and 0.206 C m^{-2} for saturation polarization and 0.026 and 0.015 for remnant polarization, which correspond to moderate energy storage density and efficiency values. The maximum energy storage density and efficiency values are summarized in Table 1. A maximum energy storage density of 4.14 J cm^{-3} was observed for the $x = 0.1$ composition at 18 kV mm^{-1}, with a recoverable energy density of 2.35 J cm^{-3}, corresponding to an efficiency of only 56.8%, while for composition $x = 0.5$, a high efficiency of 79.0% is attained but with a relatively modest energy storage density of 1.73 J cm^{-3}.

Fig. S4 shows *P-E/I-E* loops for the $x = 0.2$ composition under high applied electric fields at 200 °C. The *P-E* loop significantly narrows at the higher temperature, associated with the easier switching behavior of the polar nano-regions at this temperature. Four current peaks are observed at ca. ± 7 kV mm^{-1} at 200 °C, indicative of a reversible field induced transition. In contrast, at room temperature, the current peaks in Fig. 5 are much broader with two occurring at ca. ± 5 kV mm^{-1} and another two at ca. ± 18 kV mm^{-1}, indicative of more sluggish switching in the larger polar regions present at this temperature. At low temperature, below T_d, the polar regions are relatively large in size, and after removal of the electric field, only partially reverse back to the original state, which results in greater remnant polarization. At temperatures above T_d, the polar regions are smaller (nanoscale) and highly active allowing for electric field induced phase transitions to occur more easily with a reversal back to the original state on removal of the electric field readily occurring, resulting in lower remnant polarization.

4. Conclusions

A systematic study of B site substitution in BNT has been carried out in the system $Bi_{0.5}Na_{0.5}Ti_{1-x}(Mg_{1/3}Nb_{2/3})_xO_3$. A single cubic perovskite structure was observed for compositions with $x < 0.8$. Despite the appearance of a secondary pyrochlore phase in compositions with $x \geq 0.8$, the near linear behavior of the unit cell volume with composition indicates a complete solid solution. Although XRD analysis did not show significant structural change with temperature for the $x = 0.2$ composition, non-linear behavior in the thermal expansion of the unit cell is seen at temperatures between T_d and T_m associated with anomalies seen in the dielectric spectra. This is attributed to changes in the polar regions which are embedded in the non-polar cubic matrix, which on increasing temperature increase in number, but reduce in size, resulting in greater disorder with an accompanying volume expansion. This results in easier switching above T_d and is reflected in the *P-E* and *I-E* behavior.

Compositions with higher titanium concentration exhibit higher energy storage but show high energy loss. A maximum energy storage density of 4.14 J cm^{-3}, with a recoverable energy density of 2.35 J cm^{-3}, was obtained for the $x = 0.1$ composition. The $x = 0.5$ composition appears to have the best balance between energy storage and low energy loss, with values of 2.19 J cm^{-3} and 0.46 J cm^{-3}, respectively, corresponding to a recoverable energy density of 1.73 J cm^{-3}. Thus, when considering co-substitution as a method for improving dielectric properties a balance has to be struck between efficiency and energy storage density.

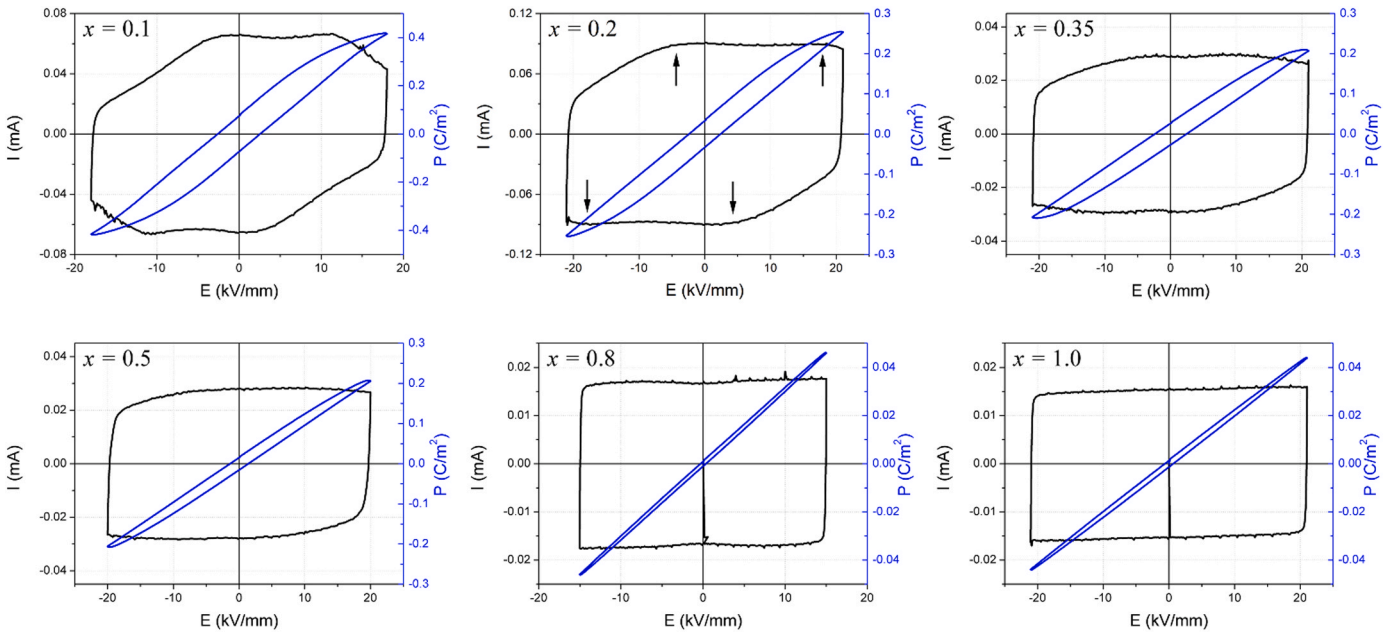

Fig. 6. P-E and I-E loops for the studied compositions in the $Bi_{0.5}Na_{0.5}Ti_{1-x}(Mg_{1/3}Nb_{2/3})_xO_3$ system measured at 10 Hz.

Table 1
Energy storage densities and efficiencies for compositions in the $Bi_{0.5}Na_{0.5}Ti_{1-x}(Mg_{1/3}Nb_{2/3})_xO_3$ system calculated from plots in Fig. 6.

x	Recoverable energy (J cm^{-3})	Energy loss (J cm^{-3})	Total charging energy (J cm^{-3})	Applied electric field (kV mm^{-1})	Energy storage efficiency (%)
0.1	2.35	1.79	4.14	18	56.8
0.2	1.93	0.99	2.92	21	66.1
0.35	1.80	0.83	2.63	21	68.4
0.5	1.73	0.46	2.19	20	79.0
0.8	0.33	0.03	0.36	15	91.7
1.0	0.44	0.04	0.48	21	91.7

CRediT authorship contribution statement

Hangfeng Zhang: Investigation, Writing – original draft. **Haixue Yan**: Conceptualization, Writing – review & editing, Supervision. **Isaac Abrahams**: Conceptualization, Writing – review & editing, Supervision.

Declaration of Competing Interest

The authors declare that they have no known competing financial interests or personal relationships that could have appeared to influence the work reported in this paper.

Data Availability

Data will be made available on request.

Acknowledgement

The authors are grateful to the Materials Research Institute at Queen Mary for studentship funding for Hangfeng Zhang.

Appendix A. Supporting information

Supplementary data associated with this article can be found in the online version at doi:10.1016/j.jallcom.2023.172385.

References

[1] M.S. Whittingham, Materials challenges facing electrical energy storage, MRS Bull. 33 (2008) 411–419, https://doi.org/10.1557/mrs2008.82.
[2] B. Jaffe, R.S. Roth, S. Marzullo, Properties of piezoelectric ceramics in the solid-solution series lead titanate-lead zirconate-lead oxide: tin oxide and lead titanate-lead hafnate, J. Res. Natl. Bur. Stand 55 (1955) (1934) 239, https://doi.org/10.6028/jres.055.028.
[3] E. Cross, Lead-free at last, Nature 432 (2004) 666–668, https://doi.org/10.1111/iwj.12889.
[4] S.-E. Park, T.R. Shrout, Ultrahigh strain and piezoelectric behavior in relaxor based ferroelectric single crystals, J. Appl. Phys. 82 (1997) 1804–1811, https://doi.org/10.1063/1.365983.
[5] W.Y. Pan, W.Y. Gu, D.J. Taylor, L.E. Cross, Large piezoelectric effect induced by direct current bias in PMN: PT relaxor ferroelectric ceramics, Jpn. J. Appl. Phys. 653 (1989) 653–661, https://doi.org/10.1143/JJAP.28.653.
[6] M. Roth, E. Mojaev, E. Dul'kin, P. Gemeiner, B. Dkhil, Phase transition at a nanometer scale detected by acoustic emission within the cubic phase Pb(Zn1/3Nb2/3)O3-xPbTiO3 relaxor ferroelectrics, Phys. Rev. Lett. 98 (2007) 1–4, https://doi.org/10.1103/PhysRevLett.98.265701.
[7] V.V. Shvartsman, D.C. Lupascu, Lead-free relaxor ferroelectrics, J. Am. Ceram. Soc. 95 (2012) 1–26, https://doi.org/10.1111/j.1551-2916.2011.04952.x.
[8] X. Tan, C. Ma, J. Frederick, S. Beckman, K.G. Webber, The antiferroelectric ↔ ferroelectric phase transition in lead-containing and lead-free perovskite ceramics, J. Am. Ceram. Soc. 94 (2011) 4091–4107, https://doi.org/10.1111/j.1551-2916.2011.04917.x.
[9] P.E.R. Blanchard, S. Liu, B.J. Kennedy, C.D. Ling, Z. Zhang, M. Avdeev, L.-Y. Jang, J.-F. Lee, C.-W. Pao, J.-L. Chen, Studying the effects of Zr-doping in (Bi 0.5 Na 0.5) TiO 3 via diffraction and spectroscopy, Dalt. Trans. 43 (2014) 17358–17365, https://doi.org/10.1039/C4DT02520B.
[10] B. Noheda, D.E. Cox, G. Shirane, J. Gao, Z.G. Ye, Phase diagram of the ferroelectric relaxor (1-x)$PbMg_{1/3}Nb_{2/3}O_3$-$xPbTiO_3$, Phys. Rev. B. 66 (2002), 054104, https://doi.org/10.1103/PhysRevB.66.054104.
[11] A.C. Larson, R.B. Dreele, (1987) Los Alamos National Laboratory Report. No. LAUR-86–748.
[12] H. Zhang, B. Yang, A.D. Fortes, H. Yan, I. Abrahams, Structure and dielectric properties of double A-site doped bismuth sodium titanate relaxor ferroelectrics for high power energy storage applications, J. Mater. Chem. A 8 (2020) 23965–23973, https://doi.org/10.1039/d0ta07772k.
[13] G. Viola, T. Saunders, X. Wei, K.B. Chong, H. Luo, M.J. Reece, H. Yan, Contribution of piezoelectric effect, electrostriction and ferroelectric/ferroelastic switching to strain-electric field response of dielectrics, J. Adv. Dielectr. 03 (2013), 1350007, https://doi.org/10.1142/S2010135×13500070.
[14] H. Binh Nguyen, L. Norén, Y. Liu, R.L. Withers, X. Wei, M.M. Elcombe, The disordered structures and low temperature dielectric relaxation properties of two misplaced-displacive cubic pyrochlores found in the Bi2O3-MIIO-Nb2O5(M=Mg, Ni) systems, J. Solid State Chem. 180 (2007) 2558–2565, https://doi.org/10.1016/j.jssc.2007.07.003.
[15] R.D. Shannon, Revised effective ionic radii and systematic studies of interatomie distances in halides and chaleogenides, Acta Crystallogr A32 (1976) 751–767, https://doi.org/10.1107/S0567739476001551.

[16] S.L. Swartz, T.R. Shrout, Fabrication of perovskite lead magnesium niobate, Mater. Res. Bull. 17 (1982) 1245–1250, https://doi.org/10.1016/0025-5408(82)90159-3.
[17] D. Schütz, M. Deluca, W. Krauss, A. Feteira, T. Jackson, K. Reichmann, Lone-pair-induced covalency as the cause of temperature- and field-induced instabilities in bismuth sodium titanate, Adv. Funct. Mater. 22 (2012) 2285–2294, https://doi.org/10.1002/adfm.201102758.
[18] B. Parija, S.K. Rout, L.S. Cavalcante, A.Z. Simões, S. Panigrahi, E. Longo, N. C. Batista, Structure, microstructure and dielectric properties of 100−x (Bi0.5Na0.5)TiO3−x[SrTiO3] composites ceramics, Appl. Phys. A. 109 (2012) 715–723, https://doi.org/10.1007/s00339-012-7105-1.
[19] J. Wu, H. Zhang, N. Meng, V. Koval, A. Mahajan, Z. Gao, D. Zhang, H. Yan, Perovskite Bi0.5Na0.5TiO3-based materials for dielectric capacitors with ultrahigh thermal stability, Mater. Des. 198 (2021), 109344, https://doi.org/10.1016/j.matdes.2020.109344.
[20] B.K. Barick, K.K. Mishra, A.K. Arora, R.N.P. Choudhary, D.K. Pradhan, Impedance and Raman spectroscopic studies of (Na0.5Bi 0.5)TiO3, J. Phys. D. Appl. Phys. 44 (2011), https://doi.org/10.1088/0022-3727/44/35/355402.
[21] Q. Xu, Z. Song, W. Tang, H. Hao, L. Zhang, M. Appiah, M. Cao, Z. Yao, Z. He, H. Liu, Ultra-wide temperature stable dielectrics based on Bi0.5Na0.5TiO3-NaNbO3 system, J. Am. Ceram. Soc. 98 (2015) 3119–3126, https://doi.org/10.1111/jace.13693.
[22] A.K. Jonscher, Dielectric relaxation in solids, J. Phys. D. Appl. Phys. 32 (1999) R57–R70, https://doi.org/10.1088/0022-3727/32/14/201.
[23] N. Meng, X. Ren, X. Zhu, J. Wu, B. Yang, F. Gao, H. Zhang, Y. Liao, E. Bilotti, M. J. Reece, H. Yan, Multiscale understanding of electric polarization in poly (vinylidene fluoride)-based ferroelectric polymers, J. Mater. Chem. C. 8 (2020) 16436–16442, https://doi.org/10.1039/d0tc04310a.
[24] M. Zhang, Z. Chen, Y. Yue, T. Chen, Z. Yan, Q. Jiang, B. Yang, M. Eriksson, J. Tang, D. Zhang, Z. Shen, I. Abrahams, H. Yan, Terahertz reading of ferroelectric domain wall dielectric switching, ACS Appl. Mater. Interfaces (2021), https://doi.org/10.1021/acsami.1c00523.
[25] M. Zhang, H. Zhang, Q. Jiang, F. Gao, R. Chen, D. Zhang, M.J. Reece, B. Yang, G. Viola, H. Yan, Terahertz characterization of lead-free dielectrics for different applications, ACS Appl. Mater. Interfaces 13 (2021) 53492–53503, https://doi.org/10.1021/acsami.1c14583.
[26] V.L. Gurevich, A.K. Tagantsev, Advances in physics intrinsic dielectric loss in crystals, Adv. Phys. 40 (1991) 719–767.
[27] C. Ma, X. Tan, E. Dul'Kin, M. Roth, Domain structure-dielectric property relationship in lead-free (1-x) (Bi1/2Na1/2) TiO3- x BaTiO3ceramics, J. Appl. Phys. 108 (2010), https://doi.org/10.1063/1.3514093.
[28] M. Zhang, X. Xu, Y. Yue, M. Palma, M.J. Reece, H. Yan, Multi elements substituted Aurivillius phase relaxor ferroelectrics using high entropy design concept, Mater. Des. 200 (2021), 109447, https://doi.org/10.1016/j.matdes.2020.109447.
[29] W. Xiong, H. Zhang, S. Cao, F. Gao, P. Svec, J. Dusza, M.J. Reece, H. Yan, Low-loss high entropy relaxor-like ferroelectrics with A-site disorder, J. Eur. Ceram. Soc. 41 (2021) 2979–2985, https://doi.org/10.1016/j.jeurceramsoc.2020.11.030.
[30] H.S. Shulman, M. Testorf, D. Damjanovic, N. Setter, Microstructure, electrical conductivity, and piezoelectric properties of bismuth titanate, J. Am. Ceram. Soc. 79 (1996) 3124–3128, https://doi.org/10.1111/j.1151-2916.1996.tb08086.x.
[31] J. Wu, A. Mahajan, L. Riekehr, H. Zhang, B. Yang, N. Meng, Z. Zhang, H. Yan, Perovskite Srx(Bi1−xNa0.97−xLi0.03)0.5TiO3 ceramics with polar nano regions for high power energy storage, Nano Energy 50 (2018) 723–732, https://doi.org/10.1016/j.nanoen.2018.06.016.
[32] C. Xu, D. Lin, K.W. Kwok, Structure, electrical properties and depolarization temperature of (Bi0.5Na0.5)TiO3-BaTiO3lead-free piezoelectric ceramics, Solid State Sci. 10 (2008) 934–940, https://doi.org/10.1016/j.solidstatesciences.2007.11.003.
[33] J. Wu, W. Sun, N. Meng, H. Zhang, V. Koval, Y. Zhang, R. Donnan, B. Yang, D. Zhang, H. Yan, Terahertz probing irreversible phase transitions related to polar clusters in Bi 0.5 Na 0.5 TiO 3 –based ferroelectric, Adv. Electron. Mater. 6 (2020), 1901373, https://doi.org/10.1002/aelm.201901373.
[34] P. Bonneau, P. Garnier, G. Calvarin, E. Husson, J.R. Gavarri, A.W. Hewat, A. Morell, X-ray and neutron diffraction studies of the diffuse phase transition in ceramics, J. Solid State Chem. 91 (1991) 350–361, https://doi.org/10.1016/0022-4596(91)90090-5.
[35] C. Ma, H. Guo, S.P. Beckman, X. Tan, Creation and destruction of morphotropic phase boundaries through electrical poling: a case study of lead-free (Bi1/2Na1/2) TiO3−BaTiO3 piezoelectrics, Phys. Rev. Lett. 109 (2012), 107602, https://doi.org/10.1103/PhysRevLett.109.107602.
[36] X. Liu, X. Tan, Giant strains in non-textured (Bi1/2Na1/2)TiO3-based lead-free ceramics, Adv. Mater. 28 (2016) 574–578, https://doi.org/10.1002/adma.201503768.
[37] J. Kling, X. Tan, W. Jo, H. Kleebe, H. Fuess, J. Rödel, In situ transmission electron microscopy of electric field-triggered reversible domain formation in Bi-based lead-free piezoceramics, J. Am. Ceram. Soc. 93 (2010) 2452–2455, https://doi.org/10.1111/j.1551-2916.2010.03778.x.
[38] W. Jo, J.E. Daniels, J.L. Jones, X. Tan, P.A. Thomas, D. Damjanovic, J. Rödel, Evolving morphotropic phase boundary in lead-free (Bi1/2Na1/2)TiO3–BaTiO3 piezoceramics, J. Appl. Phys. 109 (2011), 014110, https://doi.org/10.1063/1.3530737.
[39] C. Ma, X. Tan, E. Dul'kin, M. Roth, Domain structure-dielectric property relationship in lead-free (1−x)(Bi1/2Na1/2)TiO3□xBaTiO3 ceramics, J. Appl. Phys. 108 (2010), 104105, https://doi.org/10.1063/1.3514093.
[40] Z. Yao, Z. Song, H. Hao, Z. Yu, M. Cao, S. Zhang, M.T. Lanagan, H. Liu, Homogeneous/inhomogeneous-structured dielectrics and their energy-storage performances, Adv. Mater. 29 (2017), 1601727, https://doi.org/10.1002/adma.201601727.